In Vivo ^{13}Carbon Metabolic Imaging at 3T With Hyperpolarized ^{13}C-1-Pyruvate

S.J. Kohler,[1*] Y. Yen,[1] J. Wolber,[2] A.P. Chen,[3] M.J. Albers,[4] R. Bok,[3] V. Zhang,[3] J. Tropp,[1] S. Nelson,[3,4] D.B. Vigneron,[3,4] J. Kurhanewicz,[3,4] and R.E. Hurd[1]

We present for the first time dynamic spectra and spectroscopic images acquired in normal rats at 3T following the injection of ^{13}C-1-pyruvate that was hyperpolarized by the dynamic nuclear polarization (DNP) method. Spectroscopic sampling was optimized for signal-to-noise ratio (SNR) and for spectral resolution of ^{13}C-1-pyruvate and its metabolic products ^{13}C-1-alanine, ^{13}C-1-lactate, and ^{13}C-bicarbonate. Dynamic spectra in rats were collected with a temporal resolution of 3 s from a 90-mm axial slab using a dual ^{1}H-^{13}C quadrature birdcage coil to observe the combined effects of metabolism, flow, and T_1 relaxation. In separate experiments, spectroscopic imaging data were obtained during a 17-s acquisition of a 20-mm axial slice centered on the rat kidney region to provide information on the spatial distribution of the metabolites. Conversion of pyruvate to lactate, alanine, and bicarbonate occurred within a minute of injection. Alanine was observed primarily in skeletal muscle and liver, while pyruvate, lactate, and bicarbonate concentrations were relatively high in the vasculature and kidneys. In contrast to earlier work at 1.5T, bicarbonate was routinely observed in skeletal muscle as well as the kidney and vasculature. Magn Reson Med 58:65–69, 2007. © 2007 Wiley-Liss, Inc.

Key words: hyperpolarized ^{13}C; pyruvate; chemical shift imaging; in vivo metabolism; spectroscopic imaging

Historically, magnetic resonance (MR) has been a technique associated with low sensitivity, limited by small differences in energy-state populations dictated by the Boltzmann distribution. Increases in magnetic field strength provide modest improvements in the population distribution and thus the sensitivity, but the polarization at thermal equilibrium is fundamentally limited by the low nuclear gyromagnetic ratios. Applications of MRI have thus been focused on imaging the ^{1}H nucleus occurring in very high concentrations in fat and water in vivo. Clinical ^{1}H spectroscopy has been possible for metabolites in relatively high concentrations, while spectroscopy of nuclei with lower gyromagnetic ratios, and thus less favorable population distributions, has been difficult at best.

Methods to produce substantially altered population distributions or "hyperpolarization" by dynamic nuclear polarization (DNP) and other techniques have been known for a long time (1–6), but have not been applicable to in vivo studies due to the necessity of polarization at very low temperatures (1.2 K) and high fields. The recent development of techniques to achieve high polarization in the solid state and retain a high degree of polarization through fast dissolution procedures (7–9) has provided a mechanism to produce enhancements of MR signals by up to five orders of magnitude compared to thermal equilibrium at typical MR field strengths, thus providing the possibility of directly imaging metabolites of low concentration in vivo. In addition, the potential now exists for directly observing low concentrations of ^{13}C-labeled compounds in vivo and following their metabolism over short periods of time. Prior studies performed at 1.5T (10,11) have demonstrated the use of hyperpolarized ^{13}C-labeled pyruvate to directly monitor metabolism in vivo, and to observe the conversion of pyruvate to lactate and alanine over a time course of seconds in both normal and malignant tissue.

Here we report in vivo studies with hyperpolarized ^{13}C-pyruvate performed at 3T on a clinical MR scanner. The goal of this study was to evaluate 3T as a platform for hyperpolarized ^{13}C metabolic imaging. This study was designed to observe the organ-specific metabolite distributions as well as nonlocalized dynamics of metabolite production. For spectroscopic imaging, the sampling window limits were evaluated with respect to SNR and the spectral resolution of ^{13}C-1-pyruvate and its products ^{13}C-1-alanine, ^{13}C-1-lactate, and ^{13}C-bicarbonate.

MATERIALS AND METHODS

Animal Handling

All animal studies were carried out under a protocol approved by the UCSF Institutional Animal Care and Use Committee. Male Sprague-Dawley rats ranging in weight from 250 to 680 g were placed on a heated pad and anesthetized with isoflurane (2–3%). A catheter was introduced into the tail vein for the eventual intravenous administration of hyperpolarized pyruvate solution, and the rat was transferred to a heated pad in the RF coil in the MR scanner. While the rat was in the scanner, anesthesia was maintained by a continual delivery of isoflurane (1–2%) via a long tube to a cone placed over the rat's nose and mouth. The rat's vital signs (heart rate and oxygen saturation) were continually monitored. Care was taken to ensure that the body temperature was maintained at 37°C throughout the imaging procedures by maintaining a flow of heated water through the pad supporting the rat. At the end of the study, the rat was euthanized by a combination

[1]GE Healthcare, Menlo Park, California, USA.

[2]GE Healthcare, Amersham, UK.

[3]Department of Radiology, University of California–San Francisco, San Francisco, California, USA.

[4]Bioengineering Graduate Group, University of California–San Francisco/University of California–Berkeley, San Francisco, California, USA.

*Correspondence to: Susan J. Kohler, General Electric Company, 1 Research Circle, NMR Bldg., Room 139, Niskayuna, NY 12309. E-mail: susan.kohler@med.ge.com

Received 6 December 2006; revised 26 February 2007; accepted 5 March 2007.

DOI 10.1002/mrm.21253
Published online in Wiley InterScience (www.interscience.wiley.com).

of overanesthesia with isoflurane and bilateral thoracotomy.

Polarization Procedure

A mixture of ^{13}C-pyruvic acid (C1-labeled) and trityl radical (tris(8-carboxy-2,2,6,6,-tetra(methoxyethyl)benzo[1,2-d:4,5d′]bis(1,3)dithiole-4-yl)methyl sodium salt) was obtained from GE Healthcare (Oslo, Norway) and hyperpolarized by DNP by irradiation with 93.98-GHz microwaves in a field of 3.35T at approximately 1.2 K as previously described (9,10). The hyperpolarized pyruvic acid was dissolved in a sodium hydroxide solution to produce a 79-mM solution of pyruvate in 40-mM Tris buffer at a nominal pH of 7.4. This solution was injected into the rat tail vein within 20 s of removal from the polarizer at 1.2 K. Immediately after dissolution, an aliquot of the pyruvate solution was used to measure the liquid-state polarization using an in-house-built low-field NMR spectrometer. The pH of the final solution was also measured.

MR Studies

The MR scanner used for data acquisition was a commercial 3T General Electric Signa™ scanner equipped with the multinuclear spectroscopy (MNS) hardware package. The RF coil used in these experiments was a dual-tuned ^{1}H-^{13}C coil with a quadrature ^{13}C channel and linear ^{1}H channel constructed for these experiments based on a previously published design (12). The inner coil diameter was 8 cm, with a sensitive volume of 75 mm diameter and 90 mm length.

High-resolution T_2-weighted anatomical images were obtained in all three planes using a fast spin-echo (FSE) sequence. Axial and sagittal images were each acquired in 10 min with FOV = 10 cm, matrix = 192 × 192, slice thickness = 2 mm, and NEX = 6. Coronal images were acquired with FOV = 12 cm, matrix = 192 × 192, slice thickness = 1.5 mm, and NEX = 8, with a scan time of 10 min. The total imaging time required to obtain images in all three planes was thus approximately 30 min.

^{13}C dynamic studies were performed using a pulse and acquire acquisition sequence (FIDCSI; GE Healthcare, Waukesha, WI, USA) with a 5000-Hz acquisition bandwidth, 2048 points, and a nonselective RF pulse with a 5° or 10° flip angle (two studies of each). Spectra from a slab spanning approximately 90 mm of the rat's body were acquired every 3 s starting 3 s before the start of a 12-s manual injection of a 3-mL dose of 79 mM ^{13}C-pyruvate into the rat tail vein.

For spatial localization, a modified low-flip angle CSI acquisition sequence was used (modified version of FIDCSI; GE Healthcare, Waukesha, WI, USA) with 256 spectral points acquired using an acquisition bandwidth of 5000 Hz (50-ms spectral acquisition time) and a repetition time (TR) of 80 ms. A frequency-selective excitation pulse with a 10° flip angle was used to excite a 20-mm axial slice with an 80 × 80 mm FOV. The phase-encoding matrix was 16 × 16. Elliptical sampling of *k*-space was employed to eliminate the corners of *k*-space and reduce the scan time to 17 s. Chemical shift imaging (CSI) scans were started either 30 or 33 s after the start of a 12-s injection of a 3-mL dose of 79-mM pyruvate into the rat tail vein.

Data Processing

Dynamic data were zero-filled to 4096 points and apodized in the time domain with a 16-Hz Gaussian filter prior to a 1D Fourier transform. CSI data were processed with 16-Hz Gaussian apodization in the time domain and zero-filled to 512 points in the time domain and 64 × 64 points in the *k*-space domain prior to the Fourier transform. The data point corresponding to the frequency of maximum signal intensity for each metabolite was chosen to generate frequency-selective metabolite images presented as magnitude color overlays on a grayscale proton reference image. Regional spectra are the average of 4 voxels after zero-filling interpolation. SNRs were measured for CSI studies from a lactate metabolite map in which the signal level was measured from the voxel with maximum lactate signal in the kidney. The noise level was determined from the standard deviation (SD) of the signal level within the entire spatial array on a second baseline noise "metabolite map" generated from a single spectral point corresponding to a frequency approximately 20 ppm from any metabolite resonance frequencies.

RESULTS

Dynamic Studies

The goal of the dynamic studies was to provide baseline information about the time course of the delivery of injected pyruvate and its metabolic conversion. Accordingly, dynamic studies were performed on four rats. Figure 1 contains a stacked plot of the results from one of these experiments. Resonances from pyruvate (173 ppm) and its metabolic products lactate (185 ppm), alanine (178 ppm), and bicarbonate (162 ppm) were identified. Also present at 181 ppm is pyruvate hydrate, which exists in dynamic equilibrium with pyruvate but is not itself metabolically active (10). Baseline resolution was obtained for each of the observed resonances.

Figure 2 represents a graph of signal time courses of the metabolites from another dynamic study. Recognizing that each 10° flip angle RF pulse reduces the magnetization available for the following spectrum, the peak heights have been adjusted for the loss in intensity by successively multiplying the intensities by 1/cos(10). In addition, the pyruvate intensity has been scaled down by a factor of 10 for ease of plotting. The zero time point was taken to be the start of the 12-s pyruvate injection, and is approximately 15 s after the dissolution of hyperpolarized pyruvate. The pyruvate signal was typically first observed 3 s after the onset of injection and peaked approximately 12 s after its initial detection. The decrease in pyruvate signal due to T_1 relaxation and metabolic conversion was accompanied by increases in lactate, alanine, and bicarbonate, with lactate typically appearing slightly earlier than alanine. The shoulders visible on the pyruvate curve were observed in most of our studies, as were shoulders on lactate and alanine curves. The shoulders seen in the intensity curves were attributed to recirculation of metabolites through the rat's body.

CSI

CSI data were acquired for eight rats during this study. In each case a 20-mm axial slice was centered over one or both of the rat kidneys, as guided by initial proton scout images. A syringe filled with a 1.77-M solution of ^{13}C-1-lactate was placed on the rat within the RF coil to provide a reference signal. CSI data were acquired over a 17-s period starting 30 s after the onset of pyruvate injection. This imaging window was chosen to be later than the peak of the pyruvate signal but within a relatively flat region of the dynamic curves for the other metabolites. Representative data from one such study are shown in Fig. 3. Frequency-specific images or "metabolite maps" were generated at the resonance frequencies of pyruvate, lactate, alanine, and bicarbonate, and are displayed as color overlays on the 2-mm proton reference image corresponding to the center of the 20-mm ^{13}C axial slice. Each metabolite map is scaled individually and is displayed so that the region of highest signal for that particular metabolite appears red and the lowest appears black. Tissue-specific localization of the metabolites is evident in this and all of our CSI studies. The central vasculature shows the presence of all metabolites, while lactate and bicarbonate are concentrated in the kidneys, and alanine is high in the muscle and liver. A comparison of individual spectra shows that the overall accumulation of hyperpolarized substrates in the muscle is relatively low.

SNR and Polarization Level

We recorded in vivo CSI data with levels of polarization ranging from 1.8% to 14.1% as measured after dissolution but prior to injection. This collection of data afforded us the opportunity to plot SNR as a function of percent polarization, as shown in Fig. 4. A linear relationship was observed between SNR and percent polarization with injections of 3 mL of 79-mM pyruvate. Even with polarizations as low as 1.8%, lactate was observable in the kidney at 3T. From these data, it is predicted that with the normally achievable polarization level of 15–20%, studies could be done with concentrations of injected pyruvate as low as 8–10 mM.

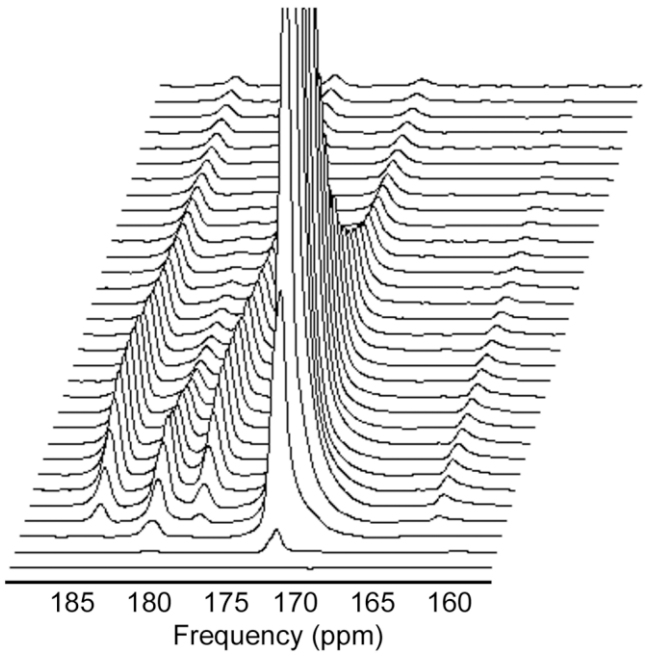

FIG. 1. Stacked plot of spectra from a dynamic study. Spectra were acquired every 3 s from a 90-mm-thick section of the rat. Lactate, pyruvate hydrate, alanine, pyruvate, and bicarbonate peaks (from left to right) are well resolved and easily identifiable. The pyruvate peak in the early spectra was truncated for ease of viewing the other metabolites.

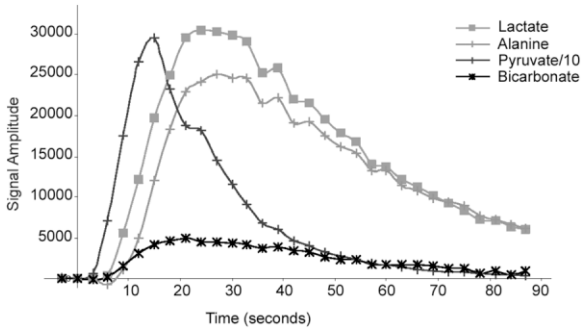

FIG. 2. Plots of metabolite signal intensities vs. time from a dynamic study similar to that of Fig. 1. The signal intensities have been corrected for the loss of magnetization caused by the use of the 10° flip angles at each excitation. Note that the signal intensities of the pyruvate peak were scaled down by a factor of 10 for plotting purposes.

DISCUSSION

Both these studies and the earlier studies at 1.5T clearly demonstrate the exciting new possibilities of observing in vivo metabolism with hyperpolarized pyruvate as a substrate, and raise the possibility of using these techniques to differentiate between normal and malignant tissue. However, there are notable differences between the 3T data and the earlier results at 1.5T (10,11). Perhaps the most striking new observation is that despite comparable pyruvate polarization levels, the sensitivity at 3T is sufficient to routinely observe a bicarbonate signal in both the dynamic scans and CSI images.

Another marked improvement at 3T was seen in the spectral resolution. In both the dynamic scans and CSI experiments, the increased spectral dispersion at 3T resulted in baseline-resolved resonances. In contrast, the published work at 1.5T reports spectra in which the alanine and pyruvate hydrate resonances are partially overlapped (10). The sparseness of the spectra at 3T suggests the possibility of shortening the sampling window to allow for a shorter total acquisition period at the expense of a decrease in spectral resolution. Since we are dealing with a hyperpolarized signal with just one "90° pulse" worth of magnetization, care must be taken in partitioning the available signal between spectral and spatial encoding. A shorter spectral acquisition window would thus provide more opportunity for spatial encoding, either to extend the in-plane spatial resolution or to extend spatial coverage to a third dimension. The trade-off is loss of SNR if the sampling window is overtruncated. The optimum sam-

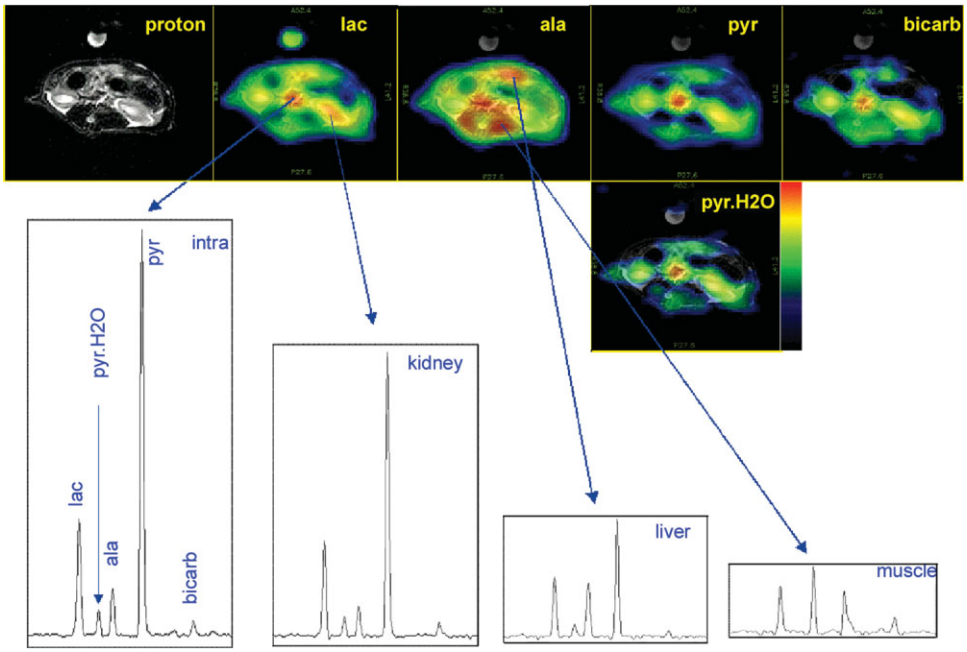

FIG. 3. Data from a CSI acquisition showing metabolite maps and individual spectra from different tissue types. Each metabolite map is scaled independently such that the highest signal level appears red and the lowest level is black. The spectra are from voxels chosen from regions of the central vasculature (intra), kidney, liver, and skeletal muscle, as indicated.

pling window is dependent on the chemical shift differences, inhomogeneous broadening (T_2*) factors, and spin-spin coupling (J_{CH}). The contributions of these effects were tested by truncating actual data collected with a 50-ms sampling window. As illustrated in Fig. 5, good in vivo separation of lactate, alanine, pyruvate hydrate, pyruvate, and bicarbonate is achievable at 3T with a sampling window as short as 12.5 ms. The lactate SNR at 25 ms is nearly equivalent to the 50-ms sampling, but drops off at 12.5 ms. This observation is consistent with lactate J_{CH}-dominated signal decay.

The dynamic studies show the conversion from pyruvate to lactate, alanine, and bicarbonate consistent with known biochemical pathways. Since the scans were done without spatial localization, the spectra represent regions of great tissue heterogeneity, and detailed mathematical modeling of the time curves to extract kinetic parameters is not warranted. However, the curves have proved to be useful in planning the CSI acquisitions.

The distribution of metabolites as shown by the CSI studies shows marked differences in distribution among the different tissue types. With the available data, differentiation between intra- and extracellular spaces is not possible, nor is it possible to differentiate between organ-specific metabolism and organ-specific retention of metabolites produced elsewhere. In any case, the distribution of metabolites is in accord with the known metabolism of the various types of tissue. For example, pyruvate in muscle serves as an energy source, leading to the production of acetyl CoA and bicarbonate under conditions of aerobic metabolism, or to the production of lactate under anaerobic conditions. In the muscle, pyruvate also serves as a

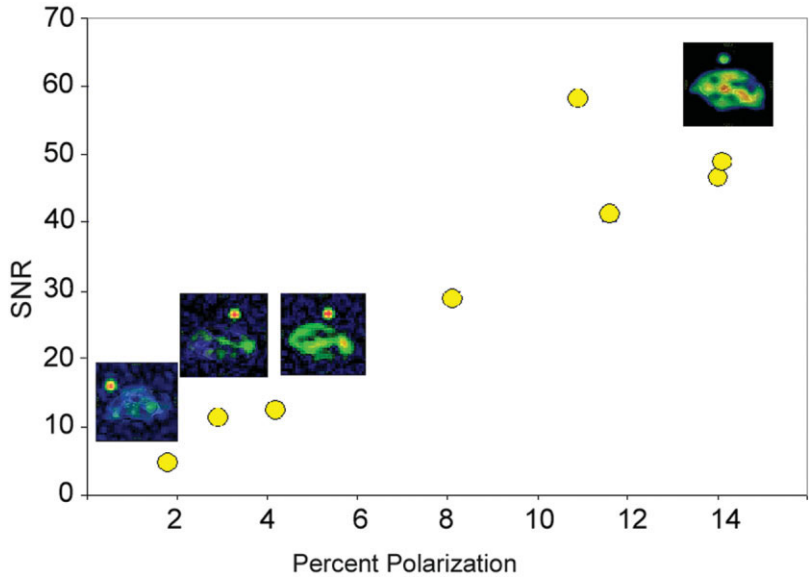

FIG. 4. Lactate SNR as a function of percent polarization. The insets are representative lactate metabolite maps at the different polarization levels.

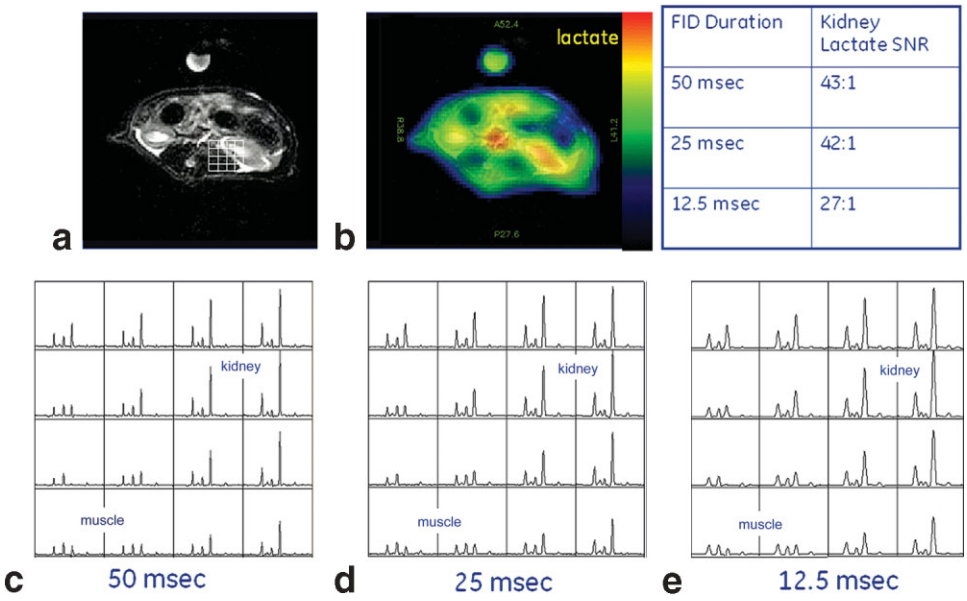

FIG. 5. Comparison of the full reconstruction of the 256-point (50 ms) data presented in Fig. 3: (**a**) anatomical ^{1}H MRI reference, and (**b**) reconstructed lactate map (50 ms). The spectral grids were reconstructed from (**c**) the full 256 data points (50 ms) and with reduced reconstructions of (**d**) 128 (25 ms) and (**e**) 64 points (12.5 ms). Note the adequate spectral separation and fidelity of the five individual ^{13}C resonances.

receptor for ammonia through transamination to alanine. Alanine and lactate in turn are transported from peripheral tissue to the liver, where they are converted to pyruvate, which is used in gluconeogenesis. It is therefore reasonable to expect relatively high alanine concentrations in liver and muscle, as observed. Lactate production is not expected to be high in non-exercising muscle. However, it is not surprising to see high levels of both lactate and bicarbonate in the highly metabolic kidney, where aerobic metabolism occurs in the cortex and anaerobic glycolysis is the source of energy for the medulla.

REFERENCES

1. Abragam A, Goldman M. Principles of dynamic nuclear polarization. Rep Prog Phys 1978;41:395–467.
2. Goldman M. Spin temperature and nuclear magnetic resonance in solids. Oxford: Oxford University Press; 1970.
3. deBoer W, Borghini M, Morimoto K, Niinikoski TO, Udo T, Low J. Dynamic polarization of protons, deuterons, and carbon-13 nuclei: thermal contact between nuclear spins and an electron spin-spin interaction reservoir. Low Temp Phys 1974;15:249–267.
4. deBoer W, Niinikoski TO. Dynamic proton polarization in propanediol below 0.5 K. Nucl Instrum Methods 1974;114:495–498.
5. Hall DA, Maus DC, Gerfen GJ, Inati SJ, Becerra LR, Dahlquist FW, Griffin RG. Polarization-enhanced NMR spectroscopy of biomolecules frozen in solution. Science 1997;276:930–932.
6. Bajaj VS, Farrar CT, Hornstein MK, Mastovsky I, Vieregg J, Bryant J, Elena B, Kreischer KE, Temkin RJ, Griffin RG. Dynamic nuclear polarization at 9T using a novel 250 GHz gyrotron microwave source. J Magn Reson 2003;160:85–90.
7. Ardenkjaer-Larsen JH, Fridlund B, Gram A, Hansson G, Hansson L, Lerche MH, Servin R, Thaning M, Golman K. Increase in signal-to-noise ratio of > 10,000 times in liquid-state NMR. Proc Natl Acad Sci USA 2003;100:10158–10163.
8. Golman K, Ardenkjaer-Larsen JH, Petersson JS, Mansson S, Leunbach I. Molecular imaging with endogenous substances. Proc Natl Acad Sci USA 2003;100:10435–10439.
9. Wolber J, Ellner F, Fridlund B, Gram A, Johannesson H, Hansson G, Hansson LH, Lerche MH, Mansson S, Servin R, Thaning M, Golman K, Ardenkjaer-Larsen JH. Generating highly polarized nuclear spins in solution using dynamic nuclear polarization. Nucl Instrum Methods Phys Res A 2004;526:173–181.
10. Golman K, in't Zandt R, Thaning M. Real-time metabolic imaging. Proc Natl Acad Sci USA 2006;103:11270–11275.
11. Golman K, in't Zandt R, Lerche M, Pehrson R, Ardenkjaer-Larsen JH. Metabolic imaging by hyperpolarized ^{13}C magnetic resonance imaging for in vivo tumor diagnosis. Cancer Res 2006;66:10855–10860.
12. Derby K, Tropp J, Hawryszko C. Design and evaluation of a novel dual-tuned resonator for spectroscopic imaging. J Magn Reson 1990;86:645–651.